Z. Phys. C – Particles and Fields 45, 501–513 (1990)

Zeitschrift für Physik C Particles and Fields

Testing QCD scaling violations in the HERA energy range

J. Blümlein[1], G. Ingelman[2]*, M. Klein[1], R. Rückl[3]

[1] Institut für Hochenergiephysik der AdW der DDR, Platanenallee 6, DDR-1615 Berlin-Zeuthen, German Democratic Republic
[2] Deutsches Elektronen-Synchrotron DESY, Notkestrasse 85, D-2000 Hamburg 52, Federal Republic of Germany
[3] Sekton Physik der Universität München, Theresientrasse 37, D-8000 München 2, Federal Republic of Germany and Max-Planck-Institut für Physik und Astrophysik, Werner Heisenberg Institut für Physik, Föhringer Ring 6, D-8000 München 40, Federal Republic of Germany

Received 23 August 1989

Abstract. High energy electron–proton colliders open new kinematical domains for the investigation of scaling violations in nucleon structure functions. Focussing on HERA as a definite study case we explore the precision which can be expected in determinations of the QCD scale parameter Λ and the running coupling constant $\alpha_s(Q^2)$. Our results provide a quantitative basis for discussions of the possibilities and requirements of QCD tests in inclusive deep inelastic scattering at HERA energies.

1 Introduction

Quantum chromodynamics (QCD) predicts logarithmic scaling violations in the nucleon structure functions [1]. The predictions can most directly be tested in deep inelastic lepton–nucleon scattering. Past fixed target experiments [2] have clearly revealed scale breaking. The observations are consistent with a logarithmic behaviour as described by the Altarelli–Parisi equations of perturbative QCD [3] for values of the scale parameter Λ around 200 MeV. Despite of the overall agreement between different experiments and theory, the measurements do however not yet provide an absolutely conclusive test of QCD. Apart from experimental difficulties, one faces a well-known basic problem. At low momentum transfer q, there are power-behaved corrections in $1/Q^2$ ($Q^2 = -q^2$) from finite mass effects and higher twist operators that complicate the QCD analysis. At sufficiently high values of Q^2, on the other hand, the $\log Q^2$ QCD effects are expected to dominate, but because of asymptotic freedom also the perturbative scaling violations shrink slowly with increasing Q^2. Fixed target experiments have covered the region from $Q^2 = \mathcal{O}(1\,\mathrm{GeV}^2)$ to a few hundred GeV^2. With the *ep* collider HERA [4], presently under construction at DESY, one will soon have new opportunities to examine scaling violations of structure functions in a kinematical domain extending two orders of magnitude in Q^2 beyond the region studied so far. This does not necessarily mean that it will be easy to put QCD to a decisive test. In any case, accurate measurements of structure functions and parton distributions at *ep* colliders are important not only with regard to QCD, but also for other physics topics such as electroweak tests or searches for new physics [5].

In this paper we examine possibilities and requirements for the QCD analysis of structure functions and quark distributions in high energy *ep* collisions. As a definite study case, we focus on HERA energies and luminosities [4]. Influences of the detector performance are also taken into account in the following sense. The QCD analysis is restricted to sections of the full available phase space where the systematic shifts of cross-sections are expected to lie below a tolerable limit. Uncertainties arising from errors in the absolute energy calibration of the calorimeters, presumably one of the most severe error sources, are estimated explicitly. Thereby, we follow studies [6] made for the H1 and ZEUS detectors [7]. In order to indicate directions of possible improvements we also consider more ideal situations where larger phase space regions are assumed to be available. For a given scenario we then evaluate the statistical precision with which the QCD scale Λ (and the running coupling $\alpha_s(Q^2)$) can be determined from QCD fits to the Q^2-dependence of structure functions. The latter are extracted [8,9] from differential *ep* cross-sections which in turn are obtained from Monte Carlo generated event samples simulating real data.

The determination of quark distributions for individual flavours or combinations of flavours from the neutral (NC) and charged current (CC) cross-

* Present address: Dept. of Radiation Sciences, Uppsala University, Box 535, S-751 21 Uppsala, Sweden

sections measureable in ep collisions is an interesting and non-trivial problem on its own [8–11]. With increasing Q^2, Z^0 exchange in the NC processes $ep \to eX$ becomes comparable in strength to γ exchange and, as a consequence, additional structure functions as well as Z^0-propagator effects enter the NC cross-sections. This leads to some complications which have not been present in past fixed target experiments. From this point of view the situation is simpler in the CC processes, $ep \to \nu X$. However, due to the non-isoscalar nature of the proton target one has four independent structure functions in the two measureable cross-sections. Strategies and prospects of extracting and separating structure functions and quark distributions have been studied in detail in earlier papers [8–10]. The results given therein are used as a starting point for the present investigations. This work also extends the study of QCD tests in [10] in different respects, in particular concerning the systematic search for structure functions suitable for QCD tests, the numerical treatment by Monte Carlo simulation and the estimates of systematic errors.

The paper is organized as follows. Section 2 provides a brief description of the theoretical cross-sections, the relevant kinematical regions and the Monte Carlo simulation of event samples. The QCD analysis of structure functions based on the Altarelli–Parisi equations is outlined in Sect. 3. Here we also summarize some previous results on the extraction of structure functions and quark distributions from the differential ep cross-sections. Our numerical estimates on the precision which can be expected in the determination of Λ from QCD fits are presented and discussed in Sect. 4. Section 5 examines the question whether the running of $\alpha_s(Q^2)$, expected in QCD, can be established at HERA. Our main conclusions are given in Sect. 6.

2 Theoretical cross-sections, kinematical regions and Monte Carlo simulation

Our analysis is based on the deep inelastic NC and CC cross-sections as calculated in the parton model to lowest order in the standard electroweak theory. The parton densities are assumed to obey leading order QCD evolution equations. As usual, the kinematics of deep inelastic scattering is described in terms of the ep squared centre-of-mass energy $s = (p_e + P)^2$, the squared momentum transfer $Q^2 \equiv -q^2 = -(p_e - p_l)^2$ and the scaling variables $y = P \cdot q / P \cdot p_e$ and $x = Q^2/2P \cdot q$. Here, p_e, p_l, P denote the four-momenta of the incoming and scattered lepton and the incoming proton, respectively. In the kinematical region $Q^2 \gtrsim 100\,\mathrm{GeV}^2$ target mass [12] and dynamical higher twist effects [13] can be neglected. Moreover, it appears sufficient to deal with four, effectively massless quark flavours (u, d, s, c) [14]. Throughout this paper, we consider unpolarized $e^{\mp}p$ scattering.

Factorizing out the dominant Q^2 dependence from the differential NC cross-sections we define the dimensionless distributions

$$\tilde{\sigma}_{\mathrm{NC}}(e^{\mp}) \equiv \frac{xQ^4}{2\pi\alpha^2 Y_+} \frac{d\sigma_{\mathrm{NC}}(e^{\mp})}{dx\,dQ^2}$$

$$= F_2(x, Q^2) \pm \frac{Y_-}{Y_+} xF_3(x, Q^2) \qquad (1)$$

where $Y_\pm \equiv 1 \pm (1-y)^2$ and α is the electromagnetic finestructure constant. The NC structure functions

$$F_2(x, Q^2) = \sum_f A_f(Q^2)[xq_f(x, Q^2) + x\bar{q}_f(x, Q^2)]$$

$$xF_3(x, Q^2) = \sum_f B_f(Q^2)[xq_f(x, Q^2) - x\bar{q}_f(x, Q^2)] \qquad (2)$$

are linear combinations of quark and antiquark density distributions, $q_f(x, Q^2)$ and $\bar{q}_f(x, Q^2)$, with flavour (denoted by the index f) and Q^2-dependent coefficients,

$$A_f(Q^2) = e_f^2 - 2e_f v_e v_f P_Z + (v_e^2 + a_e^2)(v_f^2 + a_f^2) P_Z^2$$
$$B_f(Q^2) = -2e_f a_e a_f P_Z + 4 v_e v_f a_e a_f P_Z^2. \qquad (3)$$

The latter involve the electric charges $e_f (e_u = \frac{2}{3}, e_d = -\frac{1}{3}$, etc.), and the NC vector and axial vector couplings, $v_f = (T_{3f} - 2e_f \sin^2\theta_W)/\sin 2\theta_W$ and $a_f = T_{3f}/\sin 2\theta_W$ with T_{3f} being the third component of the weak isospin ($T_{3u} = \frac{1}{2}$, $T_{3d} = -\frac{1}{2}$, etc.) and θ_W being the Weinberg angle. The Z and γ propagators enter (3) via the ratio $P_Z = Q^2/(Q^2 + m_Z^2)$.

Myltiplying the differential CC cross-section by an overall factor containing the W propagator, one is left with the following combinations of quark density distribution functions:

$$\tilde{\sigma}_{\mathrm{CC}}(e^{\mp}) \equiv \frac{4\sin^4\theta_W (Q^2 + m_W^2)^2}{\pi\alpha^2} \frac{d\sigma_{\mathrm{CC}}(e^{\mp})}{dx\,dQ^2}$$
$$= \begin{cases} \sum_i [u_i(x, Q^2) + (1-y)^2 \bar{d}_i(x, Q^2)] \\ \sum_i [\bar{u}_i(x, Q^2) + (1-y)^2 d_i(x, Q^2)] \end{cases} \qquad (4)$$

where u_i and d_i denote the up- and down-type quark flavours (u, c) and (d, s), respectively.

The above expressions cannot directly be applied to experimental data because of non-negligible higher order effects. The one-loop radiative electroweak corrections have been obtained for NC and CC scattering in complete [15] and approximate calculations [16]. We assume that the experimentally measured cross-sections can be corrected for these effects and that the QCD tests are performed with the corrected data. We have checked that excluding the region $y \gtrsim 0.9$, where the NC radiative corrections are particularly large, does not significantly change our numerical results on the precision of Λ. Furthermore, higher order QCD contributions modify the evolution

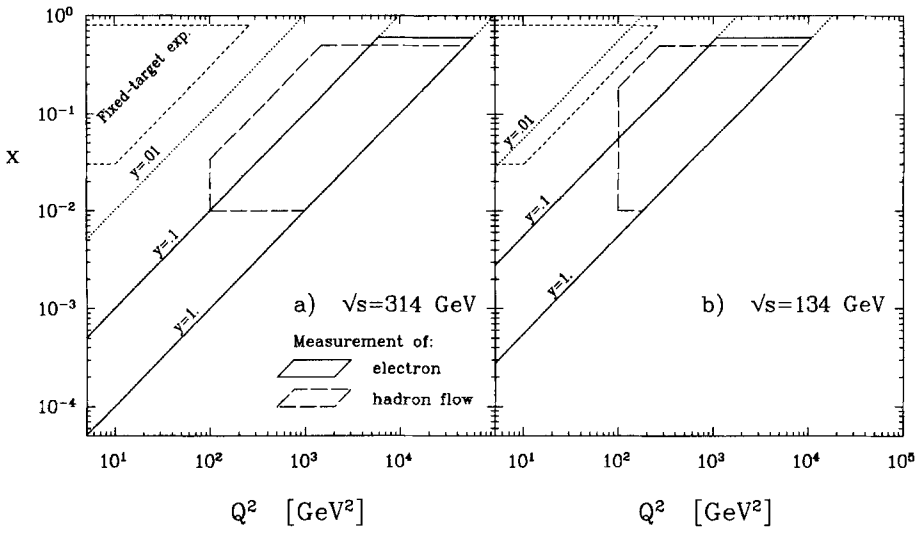

Fig. 1 a, b. Experimentally accessible regions for structure function measurements at two choices of HERA beam energies: **a** 30 GeV $e^{\mp}$ on 820 GeV proton and **b** 15 GeV $e^{\mp}$ on 300 GeV proton. The boundaries shown by full and long-dashed lines are given by (5) and (6), respectively, and specify the regions where differential cross-sections are expected to be measurable with less than 10% systematic errors based on kinematics reconstruction from the scattered electron and produced hadron flow, respectively [6]. Lines of constant y are indicated as well as the region covered by present-day fixed target experiments

equations for the parton densities [17], and generate a longitudinal structure function [18]. Since these effects have little influence on the error estimates considered here, we have neglected them. In fact, it has been shown in [10] that for $x \geqq 10^{-2}$ and $Q^2 \geqq 50\,\mathrm{GeV}^2$ at $\sqrt{s} = 314\,\mathrm{GeV}$ the neglect of the longitudinal structure function from QCD shifts the extracted value of Λ by only 20 MeV. Since this function can be determined from data at different $\sqrt{s}$ [10, 19], it can be included in the final analysis.

The kinematical regions probed at HERA energies are illustrated in Fig. 1. There are two ways to experimentally determine the kinematical variables x, y and Q^2 for a given NC event: either from the momentum of the scattered electron or the total hadron flow. However, due to finite resolution of the detectors [7] and particles escaping through the beam pipe [20] the above variables cannot be reconstructed with sufficient precision in the whole phase space. The resulting systematic shifts of the differential cross-sections can be kept below 10% in a restricted region of the phase space, which for the nominal HERA energy $\sqrt{s} = 314\,\mathrm{GeV}$, was found to be [6]
for electron measurements:

$$5 \times 10^{-5} \leqq x \leqq 0.6, \quad Q^2 \geqq 5\,\mathrm{GeV}^2, \quad y \geqq 0.1 \qquad (5)$$

for hadron measurements:

$$0.01 \leqq x \leqq 0.5, \quad Q^2 \geqq 100\,\mathrm{GeV}^2, \quad y \geqq 0.03. \qquad (6)$$

Figure 1a shows the above restrictions as boundaries in x and Q^2. The corresponding 'safe' regions at the minimum HERA energy (about $\sqrt{s} = 134\,\mathrm{GeV}$ [21]) are indicated in Fig. 1b, where we have assumed that (5, 6) still hold [22] except that $x_{\min} = Q^2_{\min}/s \simeq 3 \times 10^{-4}$. In NC events one can make use of either electron or hadron measurements, whereas CC events only allow measurements via the hadron flow. NC measurements therefore gain in accuracy through cross-checks between the two measurements and can also be extended over a larger kinematic range. Yet, a large fraction of the NC statistics is located in $0.03 < y < 0.1$ where an accurate electron measurement is not possible. Thus, the ability to measure the kinematical variables from the hadron flow is very important also for the NC case. The lower y-cut in (6) (cf. Fig. 3 below) is related to the beam pipe hole, e.g. $y = 0.01$ corresponds (for $Q^2 \geqq 100\,\mathrm{GeV}^2$) to a polar angle of the scattered quark in the range 3–5°. On the other hand, it is the electron measurement which gives access to the region of very small x in NC scattering as emphasized in Fig. 1.

Using the Monte Carlo (MC) program LEPTO [23] data samples are generated to simulate the statistics of real data. The generator is based on the standard model electroweak cross-sections given in (1–4). For the input parton distributions we use parameterization I of Duke and Owens (DO1) [24] with $\Lambda = 200\,\mathrm{MeV}$. The electroweak parameters take the values $\alpha = 1/137$, $\sin^2\theta_W = 0.226$, $m_W = 81.4\,\mathrm{GeV}$ and $m_Z = 92.5\,\mathrm{GeV}$. This choice is consistent with the standard model relations including radiative corrections.

For the main part of our analysis we assume the nominal beam energies, i.e. 30 GeV $e^{\mp}$ on 820 GeV p giving the centre-of-mass energy $\sqrt{s} = 314\,\mathrm{GeV}$. Furthermore, we concentrate on the kinematical region $Q^2 \geqq 100\,\mathrm{GeV}^2$ and $x \geqq 0.01$ where non-asymptotic scaling violations should be absent and where the log Q^2 evolution of parton densities as described by the usual Altarelli–Parisi equations in QCD [3] should be fully valid. Non-singlet fits are studied for $x \geqq 0.25$. To set the statistical scale we consider an integrated luminosity of $200\,\mathrm{pb}^{-1}$ per beam configuration which corresponds to about 150 days of fully efficient running at the design luminosity $1.5 \times 10^{31}\,\mathrm{cm}^{-2}\,\mathrm{s}^{-1}$ [4]. Measurements at $x \leqq 0.01$ may also play an important role in QCD tests

Table 1. Monte Carlo event samples and cross-sections

$\sqrt{s}$	Q^2_{min}		Restrictions	σ[pb]			
[GeV]	[GeV^2]	x-range	(5,6)	NC e^+	NC e^-	CC e^+	CC e^-
314	100	0.25 – 1	no	337	339	2.71	8.66
			yes	23.9	25.9	1.93	6.31
		0.01 – 1	no	3.72×10^3	3.74×10^3	29.4	52.7
			yes	2.37×10^3	2.40×10^3	27.2	48.4
	10	$10^{-4} - 10^{-2}$	no	4.13×10^4	4.13×10^4	4.86	5.80
			yes	2.43×10^4	2.43×10^4	—	—
134	17.8	0.25 – 1	no	2.19×10^3	2.20×10^3	1.23	5.41
			yes	143	147	0.981	4.28
		0.01 – 1	no	1.95×10^4	1.96×10^4	8.44	19.4
			yes	5.62×10^3	5.66×10^3	6.98	16.8

as pointed out in [10, 25]. Therefore, we include the region at $Q^2 \geqq 10\,\text{GeV}^2$ and $10^{-4} \leqq x \leqq 10^{-2}$ in our analysis. Here, the event rate is so large that very good statistics can be obtained with less integrated luminosity. On the theoretical side, however, the evolution equations have to be modified due to $\ln 1/x$-contributions at low x [26, 27]. It is also conceivable that non-perturbative physics [26] has some impact already at $x \simeq 10^{-4}$. The understanding of QCD in this range still requires further theoretical investigations. In order to demonstrate the statistical power available for QCD tests in the very low x region we extrapolate conventional parton densities and the leading $\log Q^2$ evolution to the region $10^{-4} \leqq x \leqq 10^{-2}$.

The MC data samples and corresponding cross-sections are summarized in Table 1 for both the full kinematical regions just described as well as for the regions restricted according to (5, 6). This shows the loss of statistics in going from an idealized situation to a more realistic one where systematic uncertainties can be kept at an acceptable level. Obviously, the most severe loss is caused by the lower cuts in y. For kinematics reconstruction based on the hadron flow this cut is essentially caused by the beam pipe hole. These limitations also lead to a gap between the kinematical region explored in fixed target experiments and the region considered suitable for accurate structure function measurements at the highest HERA energy. Since the kinematical requirements, (5) and (6), are expected [22] to remain roughly the same when lowering the centre-of-mass energy, one could decrease this gap by running at HERA with reduced beam energies. As an illustrative case, we consider the lowest practicable beam energies [21] of 15 GeV $e^{\mp}$ on 300 GeV protons yielding the c.m. energy $\sqrt{s} =$ 134 GeV (see Fig. 1b). Since the luminosity is expected to scale essentially linearly with the proton beam energy [21], we assume an integrated luminosity of only $100\,\text{pb}^{-1}$ for this low energy option.

Actually, MC events and cross-sections in each sample are recorded in bins of x and Q^2 which, in order to assure reasonable statistics, become larger as x and Q^2 increase. For Q^2 we have chosen four bins per decade which are equally large on a logarithmic scale, i.e. $\Delta \log Q^2 = 0.25$. In x we have taken bins with $\Delta x = 0.05$ for $x \leqq 0.5$, $\Delta x = 0.1$ for $0.5 \leqq x \leqq 0.8$, and the bin $0.8 \leqq x \leqq 1$. For NC events we have in some cases exploited the high statistics available at $x \leqq 0.1$ and made a finer binning with four bins per decade on a logarithmic scale.

3 Structure functions and QCD evolution

Tests of QCD scaling violations in deep inelastic scattering are performed with structure functions extracted from the inclusive differential cross-sections. In the quark-parton model, these functions are superpositions of quark and antiquark distributions with certain coefficients:

$$F(x, Q^2) = \sum_i [\alpha_i q_i(x, Q^2) + \beta_i \bar{q}_i(x, Q^2)]. \tag{7}$$

For the purpose of analysing the Q^2 evolution predicted by QCD, it is useful to separate $F(x, Q^2)$ into a non-singlet and a singlet component:

$$F(x, Q^2) = aF_{NS}(x, Q^2) + bF_S(x, Q^2) \tag{8}$$

where

$$F_{NS}(x, Q^2) = \sum_{i,j} \alpha_{ij} [q_i(x, Q^2) - \bar{q}_j(x, Q^2)] \tag{9}$$

and

$$F_S(x, Q^2) = \sum_i [q_i(x, Q^2) + \bar{q}_i(x, Q^2)]. \tag{10}$$

The latter functions obey the Altarelli–Parisi equations which, in leading logarithmic approximation, read as follows:

$$\frac{\partial}{\partial t} F_{NS}(x, t) = P_{qq}(x) \otimes F_{NS}(x, t) \tag{11}$$

$$\frac{\partial}{\partial t} \begin{pmatrix} F_S(x,t) \\ G(x,t) \end{pmatrix} = \begin{pmatrix} P_{qq}(x) & 2N_f P_{qG}(x) \\ P_{Gq}(x) & P_{GG}(x) \end{pmatrix} \otimes \begin{pmatrix} F_S(x,t) \\ G(x,t) \end{pmatrix} \tag{12}$$

with $t=(2/\beta_0)\ \ln\ [\ln\ (Q^2/\Lambda^2)/\ln\ (Q_0^2/\Lambda^2)]$, $\beta_0=11-\frac{2}{3}N_f$, Q_0^2 denoting the starting point of the Q^2 evolution, and N_f being the number of active flavours (in our case $N_f=4$). Furthermore, $G(x,Q^2)$ is the gluon density distribution, $P_{ab}(x)$ are the QCD splitting functions as given explicitly in [3], and the convolution on the right-hand side of (11, 12) is defined by

$$A(x)\otimes B(x)=\int_0^1 dx_1 \int_0^1 dx_2\,\delta(x-x_1x_2)A(x_1)B(x_2). \quad (13)$$

The initial distributions $F_{NS}(x,Q_0^2)$, $F_S(x,Q_0^2)$ and $G(x,Q_0^2)$ are neither predicted by perturbative QCD nor can they be measured in the whole x-range by a single experiment. They must therefore be fitted to the data simultaneously with the Λ parameter. Several algorithms have been developed for the QCD analysis [28–30]. Here, we mainly use the Furmanski–Petronzio program [30] in which the solution of the Altarelli–Parisi equations is obtained by expanding the input distributions at Q_0^2 and the evolution kernels in terms of orthogonal polynomials. In this way the distributions at Q_0^2 are determined by solving a system of linear equations for any Λ, which is thereafter found by a one-dimensional minimization. This method is to a large extent algebraic and rather fast on the computer as compared to non-linear multidimensional minimizations used in other algorithms. To cross-check our main results we have also made fits with the program by Abbott et al. [28].

In contrast to structure functions relevant at present fixed target energies the coefficients α_i, β_i in (7) are not constants at the high values of Q^2 reachable at ep colliders, as is clear from the NC expressions, (1–3). For example, by adding and subtracting the rescaled NC cross-sections $\tilde{\sigma}_{NC}(e^{\mp})$ one obtains

$$F_2(x,Q^2)=\tfrac{1}{2}(\tilde{\sigma}_{NC}(e^-)+\tilde{\sigma}_{NC}(e^+)) \quad (14)$$

$$xF_3(x,Q^2)=\frac{Y_+}{2Y_-}(\tilde{\sigma}_{NC}(e^-)-\tilde{\sigma}_{NC}(e^+)) \quad (15)$$

that is structure functions with Q^2 dependent coefficients $A_i(Q^2)$ and $B_i(Q^2)$ as specified in (3). While F_3 is a pure non-singlet distribution, F_2 can be decomposed into the singlet distribution F_S defined in (10) and the non-singlet distribution $\Delta_p=\sum_i(u_i+\bar{u}_i-d_i-\bar{d}_i)$:

$$F_2(x,Q^2)=\tfrac{1}{2}[A_u(Q^2)-A_d(Q^2)]x\Delta_p(x,Q^2)+\tfrac{1}{2}[A_u(Q^2)+A_d(Q^2)]xF_S(x,Q^2). \quad (16)$$

Then, using (11) and (12) it is in principle straightforward to perform QCD fits directly to the structure functions (14) and (15).

One can immediately see from (2) and (3) that xF_3 vanishes at sufficiently low Q^2, whereas F_2 reduces to the familiar electromagnetic structure function

$$F_2^{em}(x,Q^2)=\sum_i e_i^2(xq_i(x,Q^2)+x\bar{q}_i(x,Q^2)) \quad (17)$$

or, in the representation of (16),

$$F_2^{em}(x,Q^2)=\tfrac{1}{6}x\Delta_p(x,Q^2)+\tfrac{5}{18}xF_S(x,Q^2). \quad (18)$$

F_2^{em} is just one example (however, from the point of view of QCD tests the most important one) of structure functions which can be obtained from a single cross-section or a combination of cross-sections in restricted ranges of x and/or Q^2. In a similar approximate way one can extract several other distributions, in particular, valence quark distributions at $x\gtrsim 0.25$. Moreover, by using all four independent cross-sections, $\tilde{\sigma}_{NC}(e^{\mp})$ *and* $\tilde{\sigma}_{CC}(e^{\mp})$, it is possible to avoid such approximations and obtain also distributions which are not accessible otherwise. A convenient complete set of distributions obtainable from the above four cross-sections is given by the valence distributions u_v, d_v and the summed distributions $U=\sum_f(u_f+\bar{u}_f)$, $D=\sum_f(d_f+\bar{d}_f)$. Other functions can then be obtained through linear combinations of these [8, 9]. In practice this procedure requires considerably more statistics than the approximate approach and is subject to additional systematic uncertainties, for example, in the relative normalization of different data sets. Various methods for the extraction of structure functions from measured cross-sections and the accuracy which can be expected from HERA experiments are discussed in detail in [8–10]. Here, we shall follow [9] where results are presented on

(i) the non-singlet distributions u_v, d_v, $u_v\pm d_v, e_u u_v - e_d d_v$,
(ii) the singlet distribution F_S, and
(iii) the mixed distributions $u_v+S/2=\sum_i(u_i+\bar{d}_i)$,

$d_v+S/2=\sum_i(d_i+\bar{u}_i)$, $U=\sum_i(u_i+\bar{u}_i)$, $D=\sum_i(d_i+\bar{d}_i)$, $U_{sea}=U-u_v$, $D_{sea}=D-d_v$, $S=U_{sea}+D_{sea}$, F_2^{em}.

While in [9] the focus is on the determination of the shape in x of structure functions, we concentrate here on the determination of the QCD scale parameter Λ from the Q^2-dependence of the above distributions.

4 Determination of Λ

4.1 Statistical precision

The accuracy which can be achieved in determinations of the Λ parameter from QCD fits depends on the statistical accuracy of the structure function data, the available lever arm in x and Q^2, the inherent sensitivity of the structure function to Λ and the number of initial distributions that have to be fitted simultaneously with Λ. These aspects are considered in the following analysis.

To proceed systematically, we first examine the physical sensitivity of Λ of the structure functions in

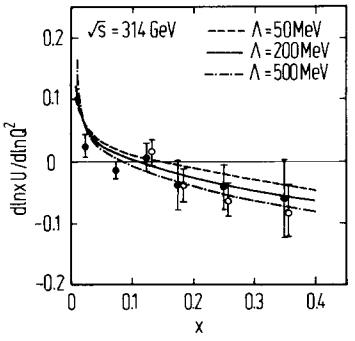

Fig. 2. Sensitivity of the distribution $xU = \sum x(u_i + \bar{u}_i)$ to the Λ parameter. The full data symbols represent MC measurements, based on $400\,\mathrm{pb}^{-1}$, within the restricted kinematical region (5, 6), while the open symbols are obtained without these cuts. The curves are theoretical predictions for different Λ values

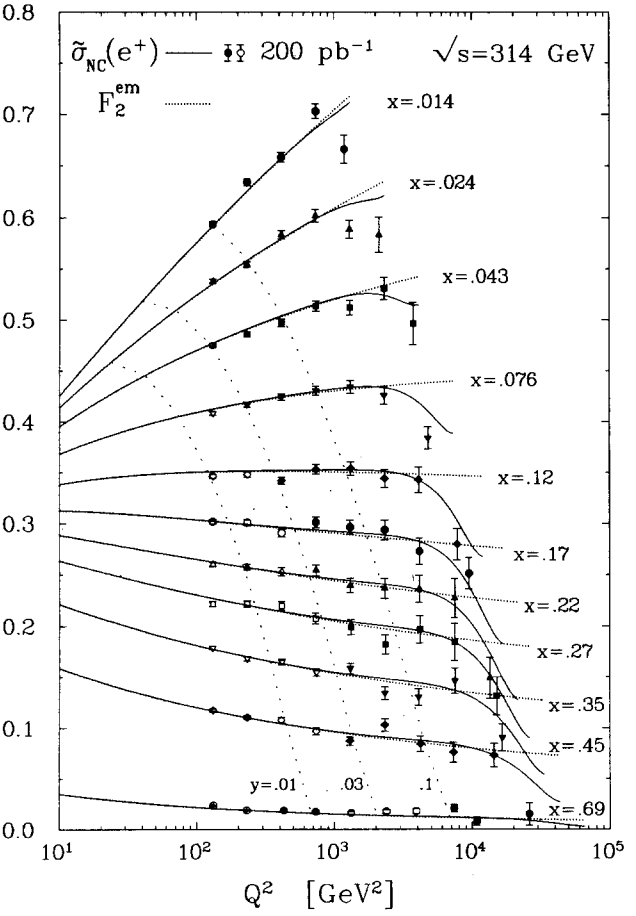

Fig. 3. Scaling violations in the differential NC e^+p cross-section at $x \geqq 0.01$. The full (open) data symbols show the results obtained with (without) the phase space restrictions of (5, 6) and correspond to $200\,\mathrm{pb}^{-1}$ at the nominal HERA energy $\sqrt{s} = 314\,\mathrm{GeV}$. The full curves are theoretical predictions on the observable, $\tilde{\sigma}_{NC}(e^+)$, represented by the MC data, while the dotted curves are the corresponding expectations on the electromagnetic structure function $F_2^{em} = \sum e_i^2 x(q_i + \bar{q}_i)$. Also shown are lines of constant y (cf. (5, 6))

comparison to their expected statistical accuracy. More specifically, following [9] we extract the distribution functions listed in the last section from the MC data sets characterized in Table 1 and calculate the logarithmic derivative $\partial \ln F / \partial \ln Q^2$. The resulting statistical errors on these derivatives are then compared with the theoretically calculated shifts due to variation of Λ from the nominal value $\Lambda = 200\,\mathrm{MeV}$ used in the MC simulation. This examination directly indicates the possible quality of a Λ measurement from a QCD analysis of a given structure function. We find that only the electromagnetic structure function F_2^{em}, (17), appears promising in this respect. In all other cases, the statistics available under the assumptions of Table 1 is not sufficient for a meaningful determination of Λ. One should note, however, that the same statistics would allow good to reasonable measurements of the shape in x of the structure functions considered in the above test. Needless to say, the study of QCD scaling violations is a much more difficult experimental problem, in particular, since the QCD evolution is rather slow from $Q^2 = 100\,\mathrm{GeV}^2$ to $Q^2 = 10^4\,\mathrm{GeV}^2$, i.e. in the typical HERA range. A good illustration of these remarks is provided by the distribution $xU = \sum_i x(u_i + \bar{u}_i)$ whose x-shape can be quite well measured (see Fig. 14a in [9]) and yet its derivative with respect to $\ln Q^2$, shown in Fig. 2, cannot be determined with sufficient accuracy for a QCD test.

In order to be more quantitative, we have also carried out a full QCD analysis for those structure functions passing the previous qualitative examination with the most favourable results. Mixed, the singlet, as well as pure non-singlet distributions have been selected. With the exception of F_2^{em}, the statistical errors on the fitted values of Λ are found to exceed 300 MeV in all cases, even when assuming a definite gluon distribution as input. This is not surprising since the bulk of the NC statistics is located at $Q^3 \leqq 10^3\,\mathrm{GeV}^2$ and $y \leqq 0.5$, where the NC cross-sections are essentially equivalent to F_2^{em}. On the other hand, structure functions based on CC data, alone or in combination with NC data, tend to be statistically more accurate at large Q^2 where the sensitivity to scaling violations is smaller.

In ep collisions, F_2^{em} can be obtained to a rather good approximation directly from the rescaled differential cross-sections $\tilde{\sigma}_{NC}(e^{\mp})$, (1), or after separation of xF_3 using the sum of $\tilde{\sigma}_{NC}(e^-)$ and $\tilde{\sigma}_{NC}(e^+)$, (14). Figure 3 shows $\tilde{\sigma}_{NC}(e^+)$ in bins of x and Q^2 as derived from the MC event sample for $\sqrt{s} = 314\,\mathrm{GeV}$ and $x \geqq 0.01$ (see Table 1). The statistical errors correspond to an integrated luminosity of $200\,\mathrm{pb}^{-1}$. Furthermore, the full curves in Fig. 3 are the result of the appropriate theoretical calculation of $\tilde{\sigma}_{NC}(e^+)$, whereas the dotted curves represent $F_2^{em}(x, Q^2)$. As expected, $\tilde{\sigma}_{NC}(e^+)$ deviates from F_2^{em} at large Q^2 where the weak NC interactions can no longer be neglected. These deviations are exhibited in Fig. 4 in more detail for

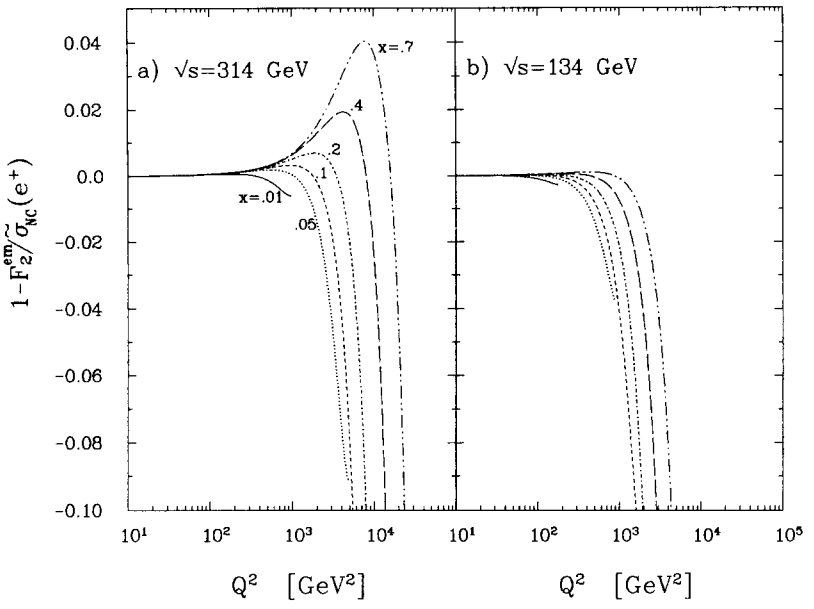

Fig. 4 a, b. Relative deviation of the structure function F_2^{em} from the actually measured quantity $\tilde{\sigma}_{NC}(e^+)$. The curves in **b** correspond to the same values of x as indicated in **a**

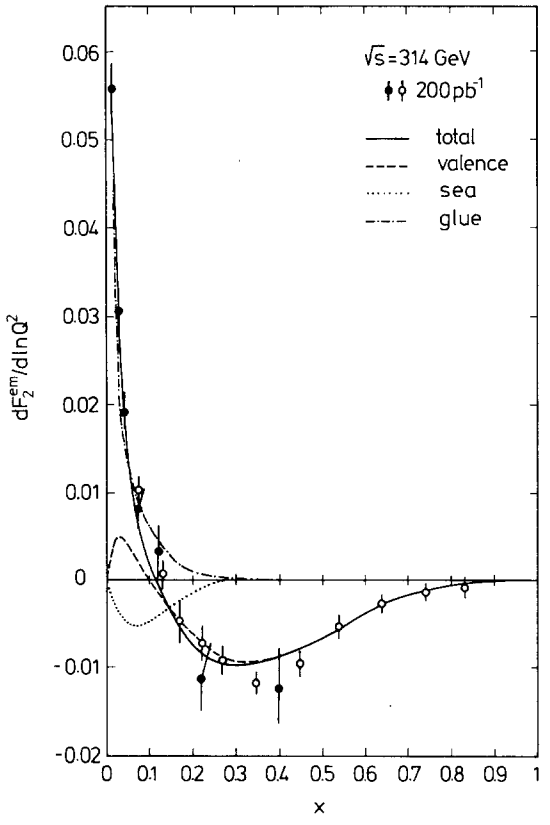

Fig. 5. Evolution of the structure function F_2^{em}. The contributions in QCD from valence quarks, sea quarks and gluons are shown separately by the curves calculated for the unrestricted y-range and $Q^2 > 100\,\text{GeV}^2$. The MC data indicate two different measurements, similarly as described in Fig. 3

both energies $\sqrt{s} = 314$ and 134 GeV. Compared with $\frac{1}{2}(\tilde{\sigma}_{NC}(e^-) + \tilde{\sigma}_{NC}(e^+))$ and $\tilde{\sigma}_{NC}(e^-)$, $\tilde{\sigma}_{NC}(e^+)$ is preferable not only as a better approximation to F_2^{em}, due to partial cancellation of Z^0 contributions in F_2 and xF_3 in (1), but also since the electroweak radiative corrections are smaller for the e^+ case [10, 15]. As can be seen from Figs. 3 and 4, some care has to be taken when performing a QCD analysis of the measured NC cross-sections. If (18) is used, the analysis should be restricted to a region in x and Q^2 where the differences of F_2^{em} and $\tilde{\sigma}_{NC}(e^{\mp})$ are small. Alternatively, one can take into account the weak effects and, for example, perform a QCD fit to $\frac{1}{2}(\tilde{\sigma}_{NC}(e^-) + \tilde{\sigma}_{NC}(e^+))$ using (16). Since the two procedures differ only in the high Q^2 region where the statistical errors are large (see Fig. 3) the error on Λ will be essentially the same for both fits. We choose the former of the two possibilities, and keep only bins in x and Q^2 where the deviations of $\tilde{\sigma}_{NC}(e^+)$ from F_2^{em} are acceptable. More definitely, requiring

$$\frac{|1 - F_2^{em}/\tilde{\sigma}_{NC}(e^+)|}{\delta_{stat}(\tilde{\sigma}_{NC}(e^+))} < \varepsilon \tag{19}$$

we have checked that for $\varepsilon \simeq 1$ the QCD fits yield stable results. At $\sqrt{s} = 314\,\text{GeV}$ and for $\int \mathscr{L}\,dt = 200\,\text{pb}^{-1}$ condition (19) excludes the region $y \geqq 0.55$, $Q^2 \geqq 2500\,\text{GeV}^2$, while at $\sqrt{s} = 134\,\text{GeV}$ and for $\int \mathscr{L}\,dt = 100\,\text{pb}^{-1}$ the region $y \geqq 0.5$, $Q^2 \geqq 1500\,\text{GeV}^2$ is excluded.

Table 2 summarizes the values of Λ and the statistical errors that result from the QCD fits to the

Table 2. Statistical precision on Λ and α_s from QCD fits to $\tilde{\sigma}_{NC}(e^+) \approx F_2^{em}$

x-range	Type of fit	Λ[MeV]	Restricted range, (5, 6) Λ[MeV]	α_s	$\langle Q^2 \rangle$[GeV^2]
a) $\sqrt{s} = 314$ GeV, $Q^2 \geqq 100$ GeV^2, $\int \mathscr{L} dt = 200$ pb^{-1}					
$x \geqq 0.25$	non-singlet, (11)	145 ± 48	175 ± 176	0.132 ± 0.023	2770
$x \geqq 10^{-2}$	(11, 12)	297 ± 76	177 ± 135	0.159 ± 0.026	400
$x \geqq 10^{-2}$	(11, 12), $xG(x, Q_0^2)$ fixed	215 ± 16	201 ± 25	0.164 ± 0.005	400
b) $\sqrt{s} = 314$ GeV, $Q^2 \geqq 10$ GeV^2, $\int \mathscr{L} dt = 100$ pb^{-1}					
$x \geqq 10^{-4}$	(11, 12)	196 ± 5	225 ± 25	0.204 ± 0.006	80
c) $\sqrt{s} = 134$ GeV, $Q^2 \geqq 18$ GeV^2, $\int \mathscr{L} dt = 100$ pb^{-1}					
$x \geqq 0.25$	non-singlet, (11)	200 ± 47	460 ± 263	0.193 ± 0.028	530
$x \geqq 10^{-2}$	(11, 12)	211 ± 27	227 ± 58	0.188 ± 0.012	160

different subsets (specified in Table 1) of the MC data plotted in Fig. 3. The χ^2 values per degree of freedom vary between 1 and 1.5 in these fits; an example is $\chi^2/\text{ndf} = 88/54$ for the case with $\sqrt{s} = 314$ GeV, $x \geqq 10^{-2}$ and restricted phase space (Table 2a). In order to check the calculated errors we have used the program of Abbott et al. [28] in the leading log version, which solves the Altarelli–Parisi equations (11, 12) numerically and applies the MINUIT minimization procedure [31] to fit Λ and the parameters of the initial distributions at Q_0^2. Compared to our main analysis we have here used numerically calculated cross-sections instead of Monte Carlo simulated ones and parameterized the input distributions (F_S, Δ, G) differently at $Q_0^2 = 10$ or 100 GeV^2 instead of 4 GeV^2. The results obtained in this way agree well with those given in Table 2. For example, we obtain $\Lambda = 192 \pm 29$ MeV instead of 201 ± 25 MeV for $x \geqq 10^{-2}$, xG fixed, and $\Lambda = 259 \pm 25$ MeV instead of 225 ± 25 MeV for $x \geqq 10^{-4}$, fitting all initial distributions. In cases with $\delta\Lambda \simeq \Lambda$, where the error estimate is less precise for a multiparameter fit, larger differences may occur using different procedures.

To discuss the results in more detail let us first concentrate on the nominal HERA energy $\sqrt{s} = 314$ GeV and the kinematical region $Q^2 \geqq 100$ GeV^2, $x \geqq 0.01$ (Table 2a). For the interpretation of the results it is useful to realize that for $x \lesssim 0.1$ the evolution of F_2^{em} is dominated by the gluon contribution, whereas for $x \gtrsim 0.25$ only the valence quarks matter, as illustrated in Fig. 5. Several comments are now in order:

(i) Fitting the three initial distributions $\Delta_p(x, Q_0^2)$, $F_S(x, Q_0^2)$ and $G(x, Q_0^2)$ simultaneously with Λ in the restricted range (5, 6) one can obtain Λ with an error $\delta\Lambda \simeq 140$ MeV.

(ii) The main obstacle for a more precise result on Λ is the unknown gluon component which plays a dominant role in the evolution of F_2^{em} (Fig. 5). If the gluon distribution were completely known a very precise value for Λ with an error of only 25 MeV could be obtained. Therefore, constraints on the gluon density from other measurements such as F_L [19] or special processes like boson-gluon fusion [32] could improve the value of $\delta\Lambda$. However, one has to proceed very carefully since the fitted value of Λ is strongly correlated with the shape of $G(x, Q_0^2)$, in particular at low x [10].

(iii) The usual way to circumvent the gluon problem is to restrict the analysis to the valence quark region, where only a non-singlet fit has to be performed. However, a fit for $x \geqq 0.25$ yields $\delta\Lambda \simeq 180$ MeV. This is mainly due to the cut $y \geqq 0.03$ which is particularly severe in the valence quark region as can be seen from Fig. 3.

(iv) Repeating the fits (i)–(iii) in the unrestricted kinematical region one obtains Λ with a statistical error $\delta\Lambda \simeq 80$, 15 and 50 MeV, respectively. These values are ideal limits corresponding to a perfect detector with full angular coverage. The comparison with the corresponding results (i)–(iii) shows the high price paid for controlling the systematic errors through the restrictions in (5, 6). On the other hand, these values also indicate the improvements that could be gained if the 'safe' region can be enlarged, but this requires a very detailed knowledge of the detectors.

So far, we have not considered the important capability to take NC data in the range $10^{-4} \leqq x \leqq$

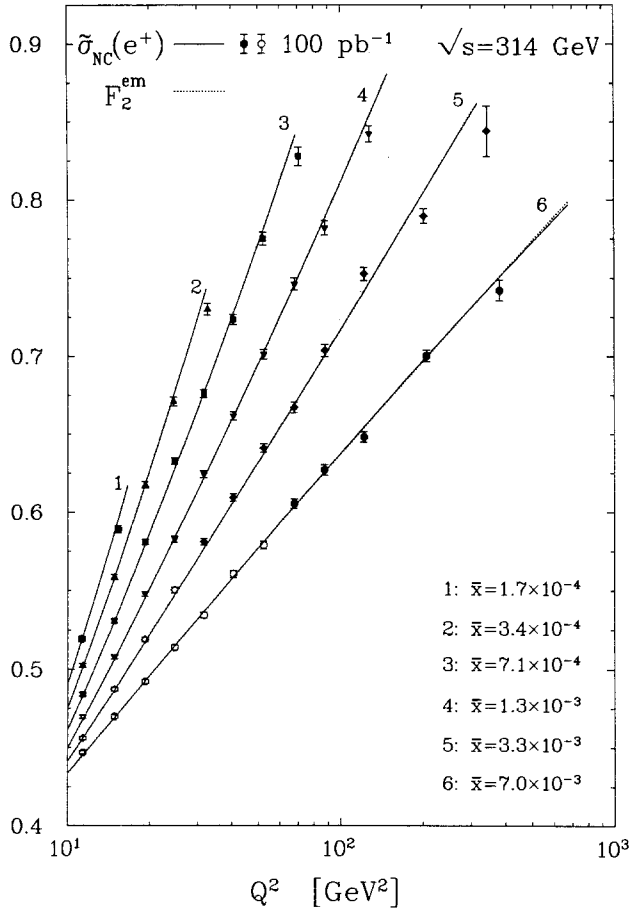

Fig. 6. Conventional leading logarithmic scaling violations in NC cross-sections extrapolated to very small values of x. The MC data and the theoretical curves are analogous to those in Fig. 3. The data correspond to an integrated luminosity of 100 pb^{-1} and cover bins in x (with boundaries at [1.0, 2.2, 4.6, 10, 22, 46, 100] × 10^{-4}) whereas the curves are calculated for the indicated mean values in x

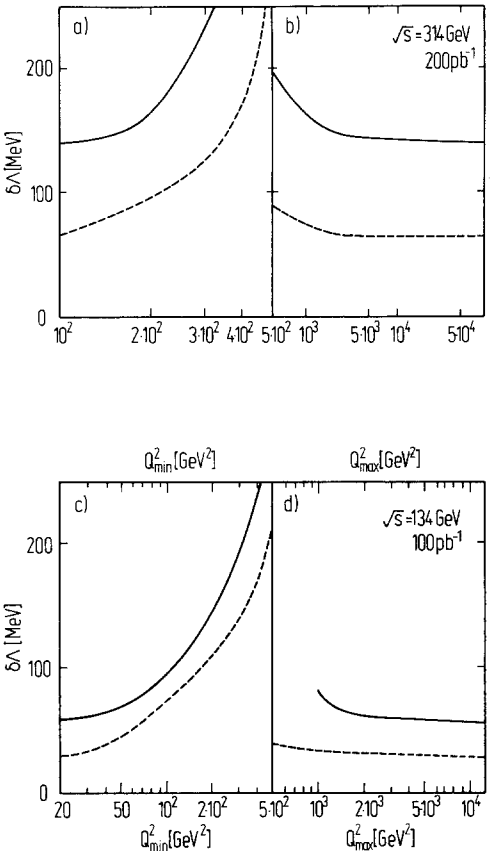

Fig. 7 a–d. Variation of the statistical error on Λ with the lower and upper limit of the Q^2 range used for the QCD fit to F_2^{em}. The full curves refer to measurements within the restricted regions defined by (5, 6), whereas the dashed curves apply to measurements without these restrictions. The condition (19) is applied in all cases. In **a** and **c** the Q^2 range extends to the maximum value consistent with these cuts, while in **b** and **d** Q^2 goes down to 100 and 18 GeV^2, respectively

10^{-2}. Here, $Q^2 \leqq 10^3$ GeV^2 and therefore γ exchange dominates completely leaving F_2^{em} as the only relevant NC structure function which, moreover, can be measured with high statistics. On the other hand, the theoretical analysis is expected to be more complicated involving the question of $\ln x$ modifications to the QCD evolution formalism [26, 27], effects of the longitudinal structure function [18], and contributions from heavy quark production [14]. Since in this paper our main interest concerns error estimates we may nevertheless, as an illustration, continue to use the ordinary evolution equations (11) and (12) also at $x < 0.01$, but keeping $Q^2 \geqq 10$ GeV^2. The corresponding MC result on $\tilde{\sigma}_{NC}(e^{\mp})$ given in Fig. 6 illustrates the strong Q^2 dependence of the structure function at low x. Even if one restricts the QCD analysis to the kinematical region, (5) and (6), one can obtain Λ with an error of only 25 MeV (Table 2b). Furthermore, at low x the Q^2 evolution of F_2^{em} is mainly determined by the gluon contribution as already mentioned (Fig. 5). Thus, the gluon density can also be better constrained in QCD fits which extend to the region $x \leqq 0.01$ [10, 25].

Another way to improve the statistical significance of Λ measurements at HERA is to lower the ep centre-of-mass energy. The reason is that the fixed lower limit in y, (5, 6), then allows access to smaller values of Q^2, see Fig. 1b, where the NC cross-section is larger and the QCD scaling violations are more pronounced. For the lowest HERA energy of about $\sqrt{s} = 134$ GeV, one can still stay in a region of Q^2 and x where the non-asymptotic background should be unimportant or at least manageable. The requirements $x > 0.01$ and $y \geqq 0.1$ imposes a minimum Q^2 value $Q^2_{min} = 18$ GeV^2. For a total luminosity of 100 pb^{-1} the MC simulation of $\tilde{\sigma}_{NC}(e^+)$ and the QCD fits have been carried out in the same way as described above for the nominal HERA energy. The resulting values of Λ are given in Table 2c. Most interestingly, we find in the case of a complete QCD fit in the restricted region defined by (5) and (6) that the statistical error on Λ decreases from $\delta\Lambda \simeq 140$ MeV at $\sqrt{s} = 314$ GeV

to $\delta\Lambda \simeq 60$ MeV at $\sqrt{s} = 134$ GeV. Thus, despite the lower integrated luminosity in this case, a factor 2 improvement is obtaind due to the larger cross-section and stronger scaling violations at lower Q^2. Further improvements can be obtaind by combining data at the two different energies. For example, a combined fit to the two data samples with $x \geqq 10^{-2}$ in Table 2a and c, respectively, gives the statistical error $\delta\Lambda = 45$ MeV.

Obviously, the inherent sensitivity of $F_2^{\text{em}}(x, Q^2)$ to Λ depends strongly on the region in Q^2 considered. One example for this assertion has just been given above. It is worthwhile to study this dependence in more detail. For definiteness, we refer to the complete QCD fits in the region $x \geqq 0.01$ at the two c.m. energies $\sqrt{s} = 314$ GeV (Table 2a) and $\sqrt{s} = 134$ GeV (Table 2c). The changes of $\delta\Lambda$ with the lower and upper limits Q^2_{min} and Q^2_{max}, respectively, are illustrated in Fig. 7. Firstly, we observe that the general behaviour of $\delta\Lambda$ is the same for the restricted and unrestricted kinematical regions. Secondly, we notice a clear difference in the influence of Q^2_{min} as compared to Q^2_{max}. The strong variation of $\delta\Lambda$ with Q^2_{min} implies that the outcome of a given fit will be mainly determined by the data at the lower end of the Q^2 region contributing to the fit. Thirdly, we find that the statistical precision of Λ is practically not influenced by measurements beyond $Q^2 \simeq$ few 10^3 GeV^2. This corroborates our earlier statement that one would not obtain a significantly more acurate value of Λ by taking the weak effects explicitly into account and including all data up to the highest accessible values of Q^2. We note, however, that for different minimum x and Q^2 values, as required for instance in the valence quark approximation, the relative weight of the very high Q^2 region can be substantially enhanced.

4.2 *Systematic shifts*

The analysis carried out in the last subsection was based on statistical considerations only. Due to the complexity of the HERA experiments a thorough investigation of all systematic problems that may influence the measurement of Λ is not possible here. However, in order to obtain some idea about the size of systematic uncertainties we shall examine consequences of errors in the calibration of the electromagnetic and hadronic calorimeters. The accurate calibration of a large calorimeter system is known to be difficult. One expects systematic errors at the per cent level [7]. These errors affect the energy measurement of the scattered electron and the produced hadrons and can therefore shift the reconstructed kinematical variables. This is an important source of systematic errors in structure function measurements. For a more detailed discussion we refer to [33, 34].

Small deviations ε_e and ε_h of the measured electron and hadron energies $\hat{E}_{e,H}$ from the actual values $E_{e,H}$, i.e. $\hat{E}_e = E_e(1+\varepsilon_e)$ and $\hat{E}_H = E_H(1+\varepsilon_h)$, cause shifts of the reconstructed kinematical variables from the electron or hadron measurements as compared to the true values:

$$\hat{x}_e = x\frac{1+\varepsilon_e}{1+\varepsilon_e-\varepsilon_e/y} \quad \hat{Q}^2_e = Q^2(1+\varepsilon_e)$$

$$\hat{y}_e = y - \varepsilon_e(1-y) \quad \hat{x}_H = x\frac{(1+\varepsilon_h)(1-y)}{1-y(1+\varepsilon_h)}$$

$$\hat{Q}^2_H = Q^2\frac{(1+\varepsilon_h)^2(1-y)}{1-y(1+\varepsilon_h)} \quad \hat{y}_H = y(1+\varepsilon_h). \tag{20}$$

Following [33] one may assume the acceptance to remain unchanged for small shifts, $\varepsilon_e, \varepsilon_h \ll 1$. In that case, the number of events per corresponding bin is identical, i.e.

$$\frac{d\hat{\sigma}(\hat{x}, \hat{Q}^2)}{d\hat{x}\, d\hat{Q}^2} d\hat{x}\, d\hat{Q}^2 = \frac{d\sigma(x, Q^2)}{dx\, dQ^2} dx\, dQ^2. \tag{21}$$

For rescaled cross-sections $\tilde{\sigma}$ such as the ones defined in (1) and (4), (21) implies

$$\hat{\tilde{\sigma}}(\hat{x}, \hat{Q}^2) = \frac{f(x, Q^2)}{f(\hat{x}, \hat{Q}^2)}\left(\frac{dx\, dQ^2}{d\hat{x}\, d\hat{Q}^2}\right)\tilde{\sigma}(x, Q^2), \tag{22}$$

where f is a factor which can be read off from the cross-section formulae and the Jacobian is calculated from (20).

Applying this procedure to the NC e^+p cross-section, we obtain the shifted differential distribution $\hat{\tilde{\sigma}}_{NC}(e^+)$. As shown in Fig. 4, the latter provides an approximate measurement of the electromagnetic structure function, i.e. $\hat{\tilde{\sigma}}_{NC}(e^+) \simeq \hat{F}_2^{\text{em}}$. Then, using the representation of F_2^{em} given in (18), we have performed QCD fits to $\hat{F}_2^{\text{em}}$ in the restricted kinematical range, (5, 6), at $\sqrt{s} = 314$ GeV. Two QCD fitting programs [30, 28] were used and consistent results were found. The net effect of small calibration errors $\varepsilon_e, \varepsilon_h$ is a shift in the location of the minimum of the χ^2 function without significant changes in its shape or normalization, i.e. the fits lead to similar χ^2 values and statistical errors $\delta\Lambda$.

The following systematic shifts were obtained for two representative cases which are dominated by the hadron flow and the electron measurements, respectively:

$\Delta\Lambda = \pm 70$ MeV for $\varepsilon_h = \pm 0.01$ in $x > 0.01$, $Q^2 > 100$ GeV^2.

$\Delta\Lambda = \mp 40$ MeV for $\varepsilon_e = \pm 0.01$ in $10^{-4} < x < 10^{-2}$, $Q^2 < 100$ GeV^2.

Furthermore, $\Delta\Lambda$ is found to vary linearly with ε. We note that the expected uncertainties in the calorimeter calibration are $\varepsilon_e = \pm 0.01$ and $\varepsilon_h = \pm 0.02$ [7].

Our results indicate a substantial influence of calibration errors on the values of Λ obtained from QCD fits above $x \simeq 0.01$. However, for QCD analyses

of measurements below $x \simeq 0.01$, the systematic effects on Λ are smaller. In both cases the systematic shifts $\Delta\Lambda$ are comparable in magnitude with the estimated statistical precision.

5 The strong coupling constant

The significance of QCD tests can be characterized by the precision with which the Λ parameter or, alternatively, the strong coupling constant α_s can be determined. As well-known, scaling violations in perturbative QCD are actually determined by the running coupling $\alpha_s(Q^2)$ which depends logarithmically on Λ and therefore is rather insensitive to Λ at large values of Q^2. It is thus clear that one can *a priori* not expect to obtain a very precise value of Λ from a measurement at high Q^2 only. On the other hand, the corresponding error on $\alpha_s(Q^2)$ can be rather small. Compared to previous measurements of α_s, HERA will cover a larger range in Q^2. Therefore, it is important to investigate whether the Q^2 dependence of α_s can be established in single experiments.

We first express the expectations on $\delta\Lambda$ presented in Table 2 in terms of the running coupling $\alpha_s(Q^2)$. To be consistent with the QCD fits, we use the relation

$$\alpha_s(Q^2) = \frac{12\pi}{25} \frac{1}{\ln(Q^2/\Lambda^2)} \tag{23}$$

which holds in leading logarithmic approximation for four massless quark flavours. As the relevant scale Q^2 we take the mean value $\langle Q^2 \rangle$ of the particular data set chosen for the analysis. The resulting values for $\alpha_s(\langle Q^2 \rangle)$ together with $\langle Q^2 \rangle$ are also included in Table 2. The statistical errors of α_s obtained by error propagation typically vary from about 5% for measurements at a relatively low mean $\langle Q^2 \rangle = \mathcal{O}(100\,\mathrm{GeV}^2)$ to about 15% for measurements at $\langle Q^2 \rangle = \mathcal{O}(10^3\,\mathrm{GeV}^2)$, assuming the luminosities stated in Table 2. One sees that there is a good chance for reasonably accurate measurements of $\alpha_s(Q^2)$ in a relatively wide range of Q^2.

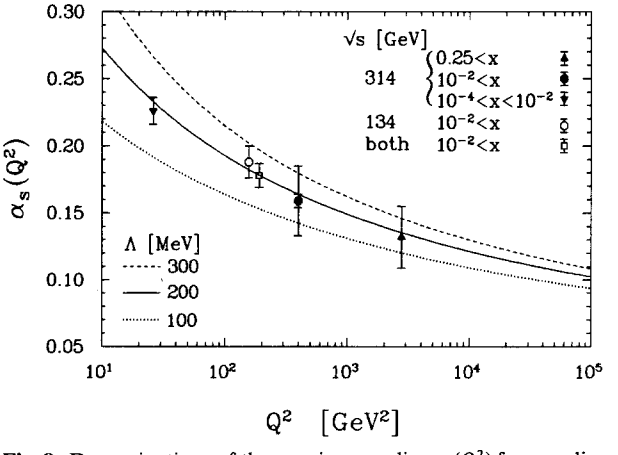

Fig. 8. Determinations of the running coupling $\alpha_s(Q^2)$ from scaling violations in F_2^{em} as explained in the text. The curves are leading order predictions on $\alpha_s(Q^2)$, (23), for different Λ values. For the two energies, $\sqrt{s} = 314$ and 134 GeV, the integrated luminosities are 200 and 100 pb^{-1}, and the lower cut in Q^2 is 100 and 18 GeV^2, respectively, with the exception of the lowest Q^2 point where $10 \leqq Q^2 \leqq 100\,\mathrm{GeV}^2$. The inner error bars for the full circle corresponds to the fit with $G(x, Q_0^2)$ fixed

To exploit this potential for testing the running of $\alpha_s(Q^2)$ one should optimize kinematical ranges and luminosities in order to obtain precise measurements at both low and high Q^2. Figure 8 contains some possible measurements of α_s at $\sqrt{s} = 314\,\mathrm{GeV}$ with 200 pb^{-1} and at $\sqrt{s} = 134\,\mathrm{GeV}$ with 100 pb^{-1}. It is obvious that the low Q^2 measurement is very important for an observation of the Q^2 variation. The cuts $x \leqq 0.01$ and $Q^2 \leqq 100\,\mathrm{GeV}^2$ were therefore imposed on the very low x data in order to lower its mean Q^2 value resulting in $\alpha_s = 0.222 \pm 0.010$ at $\langle Q^2 \rangle = 26\,\mathrm{GeV}^2$. We note that this measurement crucially relies on the understanding of QCD in the x range down to 10^{-4}. A measurement at a large mean Q^2 of a few $10^3\,\mathrm{GeV}^2$ will be possible based on the non-singlet analysis of the valence region. This fit could presumably also be optimized by using a weaker cut in (19) and pushing the upper cut in x, (5, 6), to slightly higher values although we have not attempted such a fine tuning. Nevertheless, Fig. 8 gives an indication of a running $\alpha_s(Q^2)$. The extreme Q^2 values used for the α_s measurements can be about $20\,\mathrm{GeV}^2$ and $2000\,\mathrm{GeV}^2$ giving a variation of α_s, according to (23) with $\Lambda = 200$ MeV, from 0.243 to 0.139, whereas our estimated statistical errors are about $\delta\alpha_s = 0.010$ and 0.023, respectively. The intermediate points in Fig. 8, obtained in a different kinematical range and at the lower energy, will also be important to establish a Q^2 variation. In particular, if the gluon distribution could be used as an input, the statistical error on Λ would improve substantially as indicated with the inner error bars on the full circle in Fig. 8. Finally we stress the rather high precision that can be obtained from a combined fit to data at both centre-of-mass energies, namely $\alpha_s = 0.178 \pm 0.009$ (open square in Fig. 8).

6 Summary and conclusion

We have studied the prospects for systematic QCD tests via measurements of deep inelastic structure functions in high energy ep collisions. Our starting point is a Monte Carlo simulation of the differential cross-sections for the inclusive NC and CC scattering processes, $ep \to eX$ and $ep \to \nu_e X$. Although we have mainly focussed on the nominal HERA center-of-mass energy, $\sqrt{s} = 314\,\mathrm{GeV}$, a lower energy option, $\sqrt{s} = 134\,\mathrm{GeV}$, is also considered. The corresponding integrated luminosities are taken to be 200 and 100 pb^{-1}, respectively, corresponding to 150–200 fully efficient running days for each energy and lepton beam.

From the differential cross-sections in x and Q^2, one

can extract a variety of structure functions and quark distributions. The procedures considered [8–10] involve the combination of e^-p and e^+p cross-sections, and/or simplifying approximations which, however, apply only in particular kinematical regions. Whereas the shape in x turns out to be quite accurately measurable for a number of distributions, it is only the electromagnetic structure function $F_2^{em} = \sum e_i^2 x(q_i + \bar{q}_i)$ which can be measured in x and Q^2 with the precision necessary for QCD studies. Using Monte Carlo results on F_2^{em}, we have performed various QCD fits based on the Altarelli–Parisi evolution equations in the leading logarithmic approximation. As singlet fits in large kinematical ranges are difficult to perform we have calculated the main results with two different QCD-fit programs [30, 28] and obtained consistent results. At $\sqrt{s} = 314\,\text{GeV}$ and with $x \geqq 0.01$ and $Q^2 \geqq 100\,\text{GeV}^2$, and using only the experimentally 'safe' region given by (5, 6), we obtain in an unconstrained fit of (11, 12) a statistical error for Λ of about 100 MeV. Various ways to improve the precision on Λ are pointed out:

(i) Fixing the gluon density reduces the value of $\delta\Lambda$ to about 25 MeV.
(ii) A possible extension of the kinematical region to lower y values, after a careful analysis of experimental problems, could increase the statistics considerably. For example, one would halve the error of Λ if one could include the region in y down to 0.01 [25].
(iii) Running at lower energy would reduce $\delta\Lambda$ to about 60 MeV for a luminosity $100\,\text{pb}^{-1}$ at $\sqrt{s} =$ 134 GeV, because the accessible Q^2 range then extends to smaller values where cross-sections and scaling violations are larger. As in previous fixed target experiments, a combination of data at two (or more) energies would improve the accuracy further. For the two energies considered in our study, we obtained $\delta\Lambda = 45\,\text{MeV}$.
(iv) The region of very low x values contain very high statistics data which results in a statistical error $\delta\Lambda \simeq 25\,\text{MeV}$, when formally extending the QCD leading log approximation down to $x \sim 10^{-4}$. A better understanding of QCD in this region is, however, required and further theoretical investigations needed to exploit this potential.

Another important question concerns the systematic uncertainty of Λ. A full detector simulation is beyond the scope of this paper. However, we have estimated the effects of calibration errors in the calorimetric energy measurements which are expected to be a main problem in this respect. In the standard range $x > 0.01$, $Q^2 > 100\,\text{GeV}^2$ where the kinematics can be reconstructed from the total hadron flow we find that a hadronic energy miscalibration of 1% would shift Λ by 70 MeV. In the low-x region, e.g. $x < 0.01$, $Q^2 < 100\,\text{GeV}^2$, where the kinematics is obtained from the scattered electron a corresponding 1% error in the electromagnetic calorimeters would cause the shift $\Delta\Lambda = 40\,\text{MeV}$.

Leaving aside experimental obstacles, the anticipated difficulties in the determination of Λ are in fact a matter of principle. The point is that scaling violations in QCD are determined by the running coupling $\alpha_s(Q^2)$ which at large values of Q^2 has less sensitivity to Λ. For this reason, we have reexpressed our estimates on Λ as expectations on $\alpha_s(Q^2)$. Depending on cuts in x and Q^2 one can obtain measurements of $\alpha_s(Q^2)$ at different scales ranging from $Q^2 \simeq 20\,\text{GeV}^2$ to $Q^2 \simeq 2000\,\text{GeV}^2$ with statistical errors $\delta\alpha_s/\alpha_s$ increasing from roughly 5% to 20%. The wide Q^2 range covered by a single experiment at HERA is very important for investigating the Q^2 dependence of α_s. Between the extreme values of Q^2 one expects a decrease of α_s by about 0.10 to be compared with our estimated statistical errors of about $\delta\alpha_s = 0.01$ and 0.02, respectively. Together with measurements at intermediate values of Q^2, this could give evidence for the running of the strong coupling.

To conclude we find HERA to be an interesting testing ground for QCD. The precise measurement of the Λ parameter is, however, not straightforward and requires to exploit as far as possible the potential in terms of the kinematic range, long running times, understanding QCD in the unexplored region of very low x and controlling the systematics at the one per cent level.

Acknowledgements. We are grateful to F. Eisele, J. Feltesse and T. Naumann for discussions and suggestions. One of us (J.B.) would like to thank DESY, where a large part of this work was performed, for the kind hospitality.

References

1. D.J. Gross, F. Wilczek: Phys. Rev. Lett. 30 (1973) 1343; Phys. Rev. D8 (1973) 3633; Phys. Rev. D9 (1974) 980; H.D. Politzer: Phys. Rev. Lett. 30 (1973) 1346; H. Georgi, H.D. Politzer: Phys. Rev. D9 (1974) 416
2. For reviews of deep inelastic scattering experiments see e.g. F. Eisele: Rep. Progr. Phys. 49 (1986) 233; M. Diemoz, F. Ferroni, E. Longo: Phys. Rep. 130 (1986) 293; T. Sloan, G. Smadja, R. Voss: Phys. Rep. 162 (1988) 45
3. G. Altarelli, G. Parisi: Nucl. Phys. B126 (1977) 298
4. HERA—a proposal for a large electron–proton colliding beam facility, DESY/HERA 81/10 (1981)
5. See Proc. of the HERA Workshop, Hamburg 1987, R.D. Peccei (ed.), (DESY Hamburg, 1988) Vol. 2, Chap. VI, VII
6. J. Feltess: Proc. of the HERA Workshop, Hamburg 1987, R.D. Peccei (ed.), (DESY Hamburg, 1988) Vol. 1, p. 33
7. ZEUS Collaboration: Technical proposal, DESY 1986; H1 Collaboration: Technical proposal, DESY 1986
8. G. Ingelman, R. Rückl: Phys. Lett. 201B (1988) 369; G. Ingelman, R. Rückl: Proc. of the HERA Workshop, Hamburg 1987, R.D. Peccei (ed.), (DESY Hamburg, 1988) Vol. 1, p. 107
9. G. Ingelman, R. Rückl: Z. Phys. C—Particles and Fields 44 (1989) 291
10. J. Blümlein, M. Klein, Th. Naumann, T. Riemann: Proc. of the HERA Workshop, Hamburg 1987, R.D. Peccei (ed.), (DESY Hamburg, 1988) Vol. 1, p. 67
11. M. Klein, T. Riemann: Z. Phys. C—Particles and Fields 24 (1984) 151

12. H. Georgi, H.D. Politzer: Phys. Rev. D14 (1976) 1829; R. Barnet: Phys. Rev. D14 (1976) 70
13. Y.F. Ynduráin: Quantum chromodynamics, Sects 25, 26, Berlin, Heidelberg, New York: Springer 1983; R.K. Ellis, W. Furmanski, R. Petronzio: Nucl. Phys. B212 (1983) 29
14. M. Glück, R.M. Godbole, E. Reya, Z. Phys. C—Particles and Fields 38 (1988) 441; M. Glück: Proc. of the HERA Workshop, Hamburg 1987, R.D. Peccei (ed.), (DESY Hamburg, 1988) Vol. 1, p. 119
15. D.Yu. Bardin, O.M. Fedorenko, N.M. Shumeiko: J. Phys. G7 (1981) 1331; M. Böhm, H. Spiesberger: Nucl. Phys. B294 (1987) 1081; B304 (1988) 749; D.Yu. Bardin, C. Burdik, P.Ch. Christova, T. Riemann: JINR Dubna preprint E2-87-595; H. Spiesberger: Proc. of the HERA Workshop, Hamburg 1987, R.D. Peccei (ed.), (DESY Hamburg, 1988) Vol. 2, p. 605; D.Yu. Bardin, C. Burdik, P.Ch. Christova, T. Riemann: Z. Phys. C—Particles and Fields 42 (1989) 679; Dubna preprint E2-89-145 (Z. Phys. C in press)
16. J. Kripfganz, H.J. Möhring: Z. Phys. C—Particles and Fields 38 (1988) 653; W. Beenakker, F.A. Behrends, W.L. van Neerven: to appear in the Proc. Workshop on Electroweak Radiative Corrections, Ringberg Castle, Bavaria, 1989, J.H. Kühn (ed.); J. Blümlein, Zeuthen preprint PHE 89-08 and Proc. Int. Conf. 'Frontiers in Elementary Particle Physics', Kazimierz, Poland, May 1989, Z. Ajduk, S. Pokorski (eds), Singapore: World Scientific, in press
17. A. Gonzales-Arroyo, C. Lopez, F.J. Ynduráin: Nucl. Phys. B153 (1979) 161; B159 (1979) 512; B174 (1980) 474; A. Gonzales-Arroyo, C. Lopez: Nucl. Phys. B166 (1980) 429; G. Curci, W. Furmanski, R. Petronzio: Nucl. Phys. B175 (1980) 27; W. Furmanski, R. Petronzio: Phys. Lett. 97B (1980) 437
18. M. Glück, E. Reya: Nucl. Phys. B145 (1978) 24, and references therein
19. A.M. Cooper-Sarkar, et al. Z. Phys. C—Particles and Fields 39 (1988) 281
20. H. Ziaeepour, A. Courau, V. Journé: Proc. of the HERA Workshop, Hamburg 1987, R.D. Peccei (ed), (DESY Hamburg, 1988) Vol. 1, p. 59
21. R. Brinkmann, F. Willeke: private communication
22. J. Feltesse: private communication
23. G. Ingelman: LEPTO version 5.2, DESY preprint in preparation
24. D.W. Duke, J.F. Owens: Phys. Rev. D30 (1984) 49
25. J. Blümlein, M. Klein, T. Naumann: Berlin preprint PHE-88-12 and Proc. New theories in physics, Kazimierz, Poland 1988, Z. Adjuk et al. (eds), p. 228, Singapore: World Scientific 1989
26. L.V. Gribov, E. M. Levin, M.G. Ryskin: Phys. Rep. 100 (1983) 1
27. J. Kwiecinski: Z. Phys. C—Particles and Fields 29 (1985) 561
28. L.F. Abbott, W.B. Atwood, R.M. Barnett: Phys. Rev. D22 (1980) 582
29. K. Kato, Y. Shimizu, H. Yamamoto: Progr. Theor. Phys. 63 (1980) 1295; K. Kato, Y. Shimizu: Progr. Theor. Phys. 64 (1980) 703; F.J. Yndurain: Phys. Lett. 74B (1978) 68; A. Gonzales-Arroyo et al.: in [17]; A. Devoto et al.: Phys. Rev. D27 (1983) 508; M. Virchaux, A. Oraou: Saclay preprint DPhPE 87-15; V.G. Krivokhizhim et al.: Z. Phys. C—Particles and Fields (1987) 51
30. W. Furmanski, R. Petronzio: Nucl. Phys. B195 (1982) 237
31. F. James, M. Roos: Comput. Phys. Commun. 10 (1975) 343
32. G. Barbagli, G. D'Agostini: Proc. of the HERA Workshop, Hamburg 1987, R.D. Peccei (ed.), (DESY Hamburg, 1988) Vol. 1, p. 135; S.M. Tkaczyk, W.J. Stirling: Proc. of the HERA Workshop, Hamburg 1987, R.D. Peccei (ed.), (DESY Hamburg, 1988) Vol. 1, p. 265
33. J. Feltesse: H1 internal report H1-4/85-04 (1985); F.L. Navarria, C. Zupancic, J. Feltess: Nucl. Instrum. Methods 212 (1983) 125
34. F. Brasse: Proc. of the Workshop on Experimentation at HERA, Amsterdam 1983, DESY HERA 83/20, p. 499; F. Brasse, H1 internal report H1-4/85-12 (1985)